

Enhancement of the Morphology and Open Circuit Voltage in Bilayer Polymer/Fullerene Solar Cells

Derek M. Stevens,[†] Yang Qin,[‡] Marc A. Hillmyer,[‡] and C. Daniel Frisbie*,[†]

Department of Chemical Engineering and Materials Science, University of Minnesota, 421 Washington Avenue SE, Minneapolis, Minnesota 55455, Department of Chemistry, University of Minnesota, 207 Pleasant Street SE, Minneapolis, Minnesota 55455

Received: March 11, 2009; Revised Manuscript Received: May 4, 2009

We describe the influence of thermal annealing on the performance of polymer bilayer solar cell devices of regioregular poly(3-hexylthiophene), regiorandom poly(3-hexylthiophene), or poly(3-hexyl-2,5-thienylene vinylene) (P3HTV), with C_{60} as the electron acceptor. In all cases, charge collection improves with heat treatment as the donor/acceptor layers intermix. Open circuit voltage, V_{oc} , also improves with annealing temperature, trending consistently with a reduction in the dark forward current. With extreme temperatures, C_{60} completely penetrates the polymer film, causing a reduction in V_{oc} . This C_{60} penetration in annealed devices can be prevented by inclusion of a pentacene electron-blocking layer at the anode. For P3HTV/ C_{60} solar cells, these treatments lead to peak power conversion efficiencies of 1.19%.

Introduction

Because of their promise for combining energy conversion with low-cost manufacture,^{1–3} organic solar cells have received significant research interest as a potential source of renewable energy. The best polymer^{4–7} and small molecule^{8,9} devices can now achieve power conversion efficiencies of 4–5% or more. For polymer systems, the benchmark device structure is a bulk heterojunction blend of the electron donor regioregular poly(3-hexylthiophene) (r-reg P3HT) and electron acceptor [6,6]-phenyl- C_{61} -butyric acid methyl ester (PCBM). A key advantage of r-reg P3HT over other polymers is its crystallinity, which enhances carrier mobility through extended conjugation lengths and interchain interactions.¹⁰ In addition to charge transport, however, an optimized nanoscale donor/acceptor morphology is essential for dissociating the photogenerated excitons within their diffusion length and facilitating efficient charge collection.^{1,2} Efficiency records in polymer blends have been brought on largely through morphology improvements due to changes in device processing, such as thickness, composition, casting solvent, spin-coating conditions, and thermal annealing.^{4,5,11–15}

With current peak external quantum efficiency (EQE) of more than 60%⁴ and reported internal quantum efficiencies as high as 85% or more,^{12,16} additional charge collection improvements in the well-studied bulk heterojunction systems may prove only marginal. To significantly enhance organic solar cell performance, more fundamental changes, such as the use of stacked layer tandem devices,^{7,9,17} will be required. One attractive route toward improving short circuit current, J_{sc} , is to absorb a broader fraction of the incident solar spectrum using low-band gap polymers,¹⁸ such as benzothiadiazole copolymers^{6,7,19,20} and derivatives of poly(2,7-carbazole)s^{20,21} or poly(thienylene vinylene)s (PTVs).^{22–25} With the development of such new materials, processing conditions must be re-examined. Recipes that yield near-optimal bicontinuous nanoscale network mor-

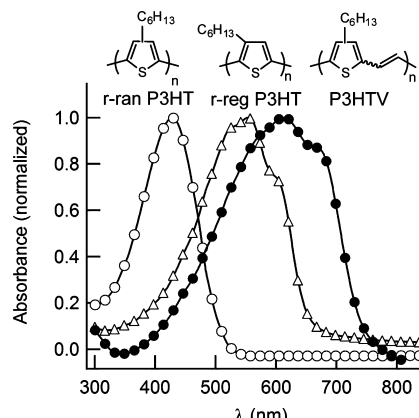


Figure 1. Chemical structures and normalized absorbance spectra of polymer thin films: r-ran P3HT (open circles), r-reg P3HT (open triangles), P3HTV (closed circles).

phologies in one system (e.g., r-reg P3HT/PCBM) may no longer be effective for each combination of new materials.

Equally important in organic solar cell efficiency is the open circuit voltage, V_{oc} , which has been found to be governed by the difference between the HOMO of the donor and LUMO of the acceptor.^{18,26} V_{oc} can also depend on various fabrication considerations, such as variation in morphology of the active layer,²⁷ choice of metal,^{26,28–30} and buffer layers at contacts.^{31,32} For example, several recent studies have shown organic or metal oxide interfacial layers can increase V_{oc} by blocking electron transport at the anode.^{33–36} Additionally, in bilayer device architectures of C_{60} with various small molecule electron donors^{37–40} as well as polymers,^{41,42} thermal annealing has been shown to increase V_{oc} . In many cases, this increase is concurrent with an increase in rectification and shift toward higher voltage in the dark forward current. In the case of polymer/ C_{60} bilayers, J_{sc} also increases with annealing temperature due to mixing between the two phases.

Here, we report on photovoltaic (PV) devices consisting of bilayers of C_{60} with three different electron donor polymers:

* Corresponding author. E-mail: frisbie@cems.umn.edu.

[†] Department of Chemical Engineering and Materials Science.

[‡] Department of Chemistry.

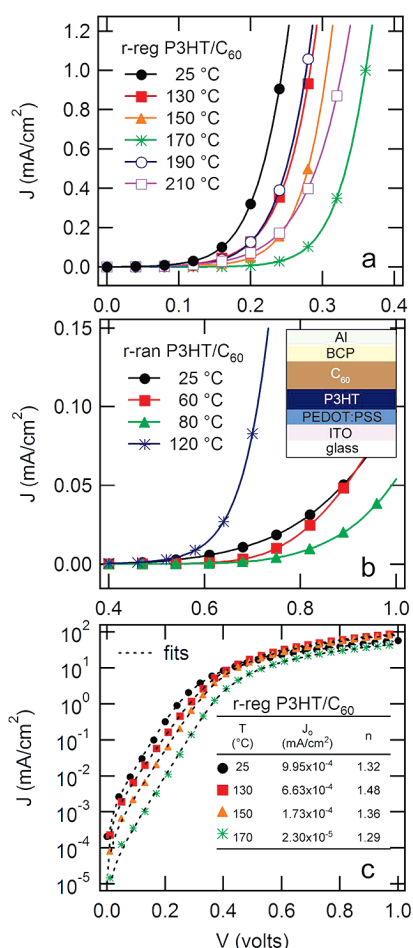


Figure 2. Dark forward current in bilayers of P3HT (34 nm)/C₆₀ (40 nm) as a function of annealing temperature after C₆₀ deposition: (a) r-reg P3HT bilayers annealed from 25 to 210 °C, (b) r-ran P3HT bilayers and schematic of device structure (inset), and (c) r-reg P3HT bilayers annealed from 25 to 170 °C. Symbols are experimental data, and the dashed lines represent fits to the data using eq 1.

r-reg P3HT; regiorandom P3HT (r-ran P3HT); and a low-band gap, soluble PTV derivative, poly(3-hexyl-2,5-thienylene vinylene) (P3HTV). Thermal annealing promotes phase mixing between the polymer and C₆₀, significantly increasing J_{sc} . For P3HTV/C₆₀ bilayers, the maximum J_{sc} and EQE obtained are, in fact, higher than previous literature reports for bulk heterojunction blends of PTVs with PCBM.^{22–25,43} In all cases, V_{oc} is also increased through intermediate annealing temperatures, concurrent with observed shifts in the dark current–voltage (J – V) characteristics. At higher temperatures, C₆₀ penetrates entirely through the polymer to the anode, shorting the device and reducing V_{oc} . We show that this penetration and subsequent drop in V_{oc} can be prevented by inserting a thin layer of pentacene below the polymer. In P3HTV/C₆₀ bilayers, combining this barrier layer with thermal annealing leads to efficiencies of 1.19%.

Experimental Methods

Materials. Regioregular P3HT ($M_n = 20.5$ kg/mol, $M_w = 35.7$ kg/mol, PDI = 1.7) and regiorandom P3HT ($M_n = 26.4$ kg/mol, $M_w = 83.0$ kg/mol, PDI = 3.1) were purchased from Rieke Metals (Lincoln, NE). P3HTV ($M_n = 4.5$ kg/mol, $M_w = 5.4$ kg/mol, PDI = 1.2) was synthesized via ADMET polymerization, the details of which will be described elsewhere.⁴⁴

C₆₀ and PCBM were purchased from American Dye Source (Baie-d'Urfé, Quebec). Bathocuproine (BCP) was purchased from Alfa Aesar (Ward Hill, MA). Poly(3,4-ethylenedioxythiophene) poly(styrenesulfonate) (PEDOT:PSS, Clevios P VP AI 4083) aqueous dispersion was purchased from H.C. Starck (Newton, MA). All solvents were purchased from Sigma-Aldrich (St. Louis, MO). All purchased materials were used as received.

Device Fabrication. Sheets of glass coated with indium tin oxide (ITO, Delta Technologies (Stillwater, MN), sheet resistance 8–12 Ω/sq) were patterned via photolithography and used as the substrate for device fabrication. Substrates were cleaned by consecutive sonifications in acetone, methanol, and isopropyl alcohol, followed by a 5 min UV–ozone treatment. PEDOT:PSS (thickness ca. 25 nm) was spin-coated onto the clean substrates, which were subsequently dried at 130 °C for 10 min to remove residual water. Devices were then moved to a nitrogen atmosphere glovebox for the balance of the fabrication process. Polymer films were spin-coated from 1,2-dichlorobenzene solutions at concentrations of 15 mg/mL (r-reg P3HT, P3HTV) or chloroform solutions at concentrations of 4 mg/mL (r-ran P3HT). Unless otherwise mentioned, final polymer film thicknesses were ~34 nm (r-reg P3HT, r-ran P3HT) and 23 nm (P3HTV). All evaporations were completed in a custom-built thermal evaporation system enclosed in a nitrogen atmosphere glovebox, operating at a base pressure of $<2 \times 10^{-6}$ Torr. The deposition rate for all organics was 0.5 Å/s, at a controlled substrate temperature of 25 °C. After spin-coating the polymer, 40 nm of C₆₀ was evaporated, followed by 10 nm of BCP.⁴⁵ Eighty nanometers of aluminum was evaporated through a shadow mask at a rate of 3.5 Å/s, defining an active area for each device of 9 mm². Annealed devices were heated for 20 min at various temperatures, always immediately after C₆₀ deposition and before BCP deposition, to prevent crystallization of the BCP.^{46–48}

Characterization. Polymer molecular weights were estimated from size exclusion chromatography in chloroform (1 mL/min) using a Hewlett-Packard (HP) 1100 system equipped with a HP 1100 autosampler, a HP 1100 HPLC pump, a HP 1047A refractive index (RI) detector and an Agilent 1200 UV–vis detector. Three styragel columns (Polymer Laboratories (Shropshire, UK); 5 μm Mix-C), which were kept in a column heater at 35 °C, were used for separation. The columns were calibrated with polystyrene standards (Polymer Laboratories). Thermal behavior of the polymers was measured on a differential scanning calorimeter from TA Instruments (New Castle, DE). Transition temperatures were taken from the second heating cycle, ramping at 10 °C/min. Polymer film thicknesses were measured with a KLA-Tencor P-16 profilometer (Milpitas, CA). Thermal evaporation rates and thicknesses were monitored using a quartz crystal microbalance (Inficon, East Syracuse, NY), which was calibrated using profilometry or spectroscopic ellipsometry (J.A. Woollam Co., Inc., Lincoln, NE). Thin film images were obtained using a Veeco Nanoscope IIIa atomic force microscope (AFM, Plainview, NY) operating in tapping mode.

UV–vis absorption measurements were performed on thin films of the polymers spin-coated onto glass substrates, and optical band gaps were determined by the absorption edge of each spectrum. Cyclic voltammetry was carried out on a 100B analyzer from BAS (West Lafayette, IN). The three-electrode system consisted of a glassy carbon disk as working electrode, a Ag wire as auxiliary electrode, and Ag/AgCl (calibrated with ferrocene^{+1/2} couple, 0.40 V vs SCE in 0.1 M [NBu₄][PF₆] acetonitrile solution⁴⁹) as the reference electrode. Polymer films

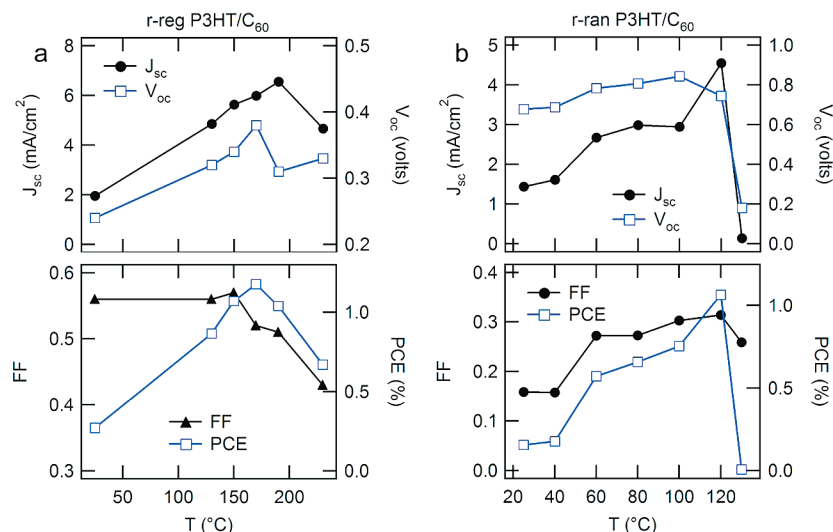


Figure 3. Summarized solar cell performance for P3HT (34 nm)/C₆₀ (40 nm) bilayers as a function of annealing temperature after C₆₀ deposition, 100 mW/cm² light intensity: (a) r-reg P3HT and (b) r-ran P3HT.

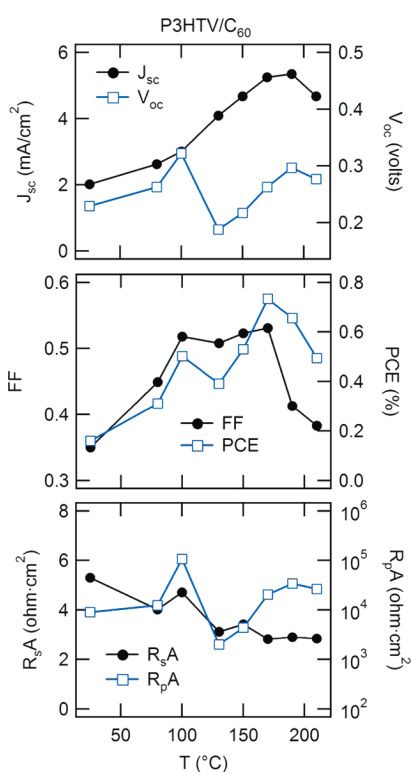


Figure 4. P3HTV (23 nm)/C₆₀ (40 nm) bilayers as a function of annealing temperature after C₆₀ deposition. Solar cell performance data are shown for 100 mW/cm² light intensity. Equivalent circuit series and shunt resistances were estimated from J-V scans in the dark.

were obtained by drop-casting solutions onto the glassy carbon electrode, and the cyclic voltammograms were recorded in CH₃CN containing [Bu₄N][PF₆] (0.1 M) as the supporting electrolyte. The redox potentials are reported relative to the saturated calomel electrode (SCE).

Device current–voltage measurements were taken on an Agilent 4155C Semiconductor Parameter Analyzer (Santa Clara, CA). The illumination source was a 150 W Xe arc lamp (Oriel) with an AM 1.5G filter. A series of neutral density filters modulated the incident light intensity, which was measured using a multifunction optical meter and broadband thermopile

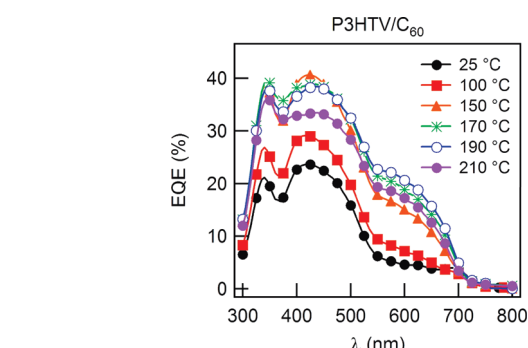


Figure 5. External quantum efficiency of P3HTV (23 nm)/C₆₀ (40 nm) bilayers as a function of annealing temperature after C₆₀ deposition.

detector (Newport, Irvine, CA). Reported solar cell data are average values over typically six devices, measured in air. Action spectra measurements for EQE were measured with a lock-in technique, using a 100 W Xe arc lamp (Oriel) illumination source in line with a 0.125 m monochromator (Newport, Cornerstone 130).

Results and Discussion

Open Circuit Voltage. Chemical structures and thin film absorbance spectra of r-reg P3HT, r-ran P3HT, and P3HTV are shown in Figure 1. The lack of regular head-to-tail repeat units in r-ran P3HT decreases the conjugation length of the polymer, leading to an absorption spectrum that is, in comparison to r-reg P3HT, blue-shifted and lacking in vibronic character.⁵⁰ P3HTV, although also consisting of a random placement of its hexyl side group, still shows vibronic structure in its absorbance and is, indeed, semicrystalline.⁴³

Table 1 summarizes the optical band gaps and HOMO levels of each polymer, as determined by cyclic voltammetry (Figure S1 of the Supporting Information).^{51,52} The data were compared against the V_{oc} obtained in PV devices under 100 mW/cm² light intensity for both unannealed bilayers with 40 nm C₆₀ as the acceptor and bulk heterojunction blends with PCBM (1:1 by weight). For both device architectures, the relationship between the polymer HOMO level and V_{oc} is essentially linear, in good general agreement with the aforementioned dependence of V_{oc}

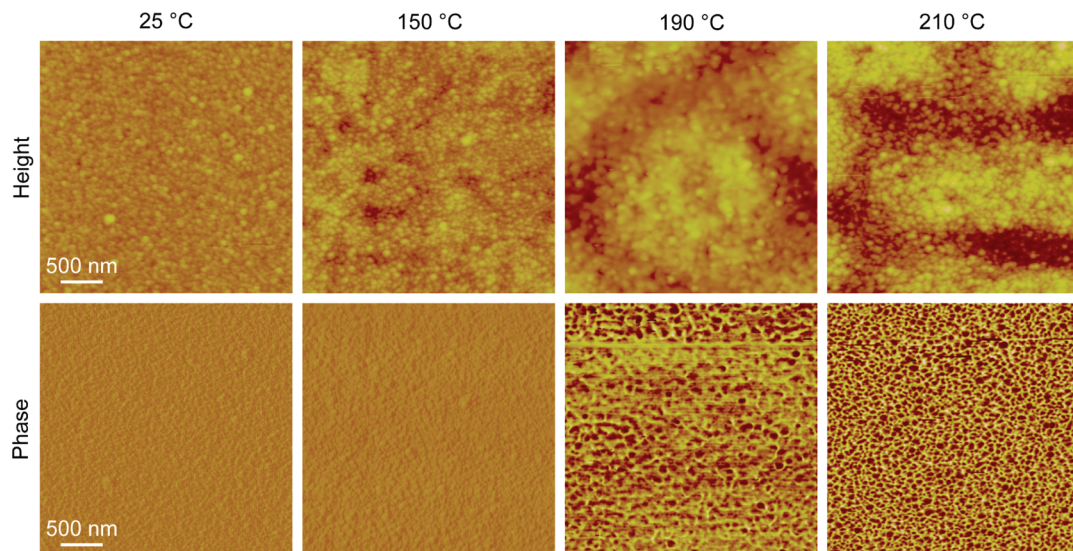


Figure 6. AFM height and phase images of P3HTV (23 nm)/C₆₀ (40 nm) bilayers annealed at different temperatures. The vertical scale is 50 nm for all height images.

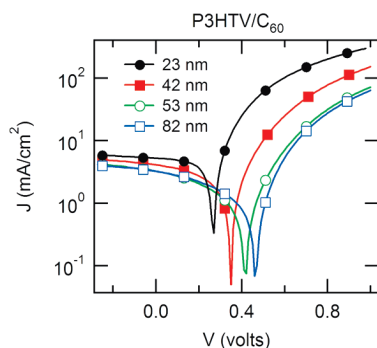


Figure 7. *J*–*V* curves of P3HTV/C₆₀ (40 nm) bilayers annealed at 170 °C under 100 mW/cm² light intensity as a function of P3HTV layer thickness.

on the difference between the HOMO of the donor and the LUMO of the acceptor. Overall, the C₆₀ bilayer *V*_{oc}'s are smaller, by 0.2–0.3 V, than what we obtain in bulk heterojunction blends with PCBM. This difference is not unexpected, given that C₆₀ has a greater electron affinity than PCBM.^{53,54}

Annealing Effects: r-reg P3HT/C₆₀ and r-ran P3HT/C₆₀. For the bilayer devices consisting of r-reg P3HT/C₆₀ and r-ran P3HT/C₆₀, significant changes in performance are observed upon annealing after C₆₀ deposition. *J*–*V* characteristics of both bilayers measured in the dark as a function of annealing temperature for a fixed time of 20 min are shown in Figure 2. For intermediate annealing temperatures, both plots shift toward higher voltages in the onset for forward current. This shift can be expressed quantitatively by a decrease in *J*_o, the reverse saturation current density of an equivalent diode. To estimate values for *J*_o as well as the equivalent circuit diode ideality factor, *n*, series resistance, *R*_s*A*, and shunt resistance, *R*_p*A*, the dark curves are fit to the following equation:^{55,56}

$$J = \frac{1}{1 + \frac{R_s A}{R_p A}} \left(J_o \left[\exp \left(\frac{q(V - R_s A J)}{n k T} \right) - 1 \right] + \frac{V}{R_p A} \right) \quad (1)$$

where *q* is the electron charge, *k* is Boltzmann's constant, and *T* is the temperature. For r-reg P3HT/C₆₀ bilayers annealed at

room temperature up to 170 °C, *J*_o decreases by almost a factor of 20, from approximately 1.0 × 10⁻³ to 2.3 × 10⁻⁵ mA/cm², as shown in Figure 2c. For the r-ran P3HT/C₆₀ bilayers, the dark *J*–*V* curves are nonideal in shape and are not well represented by eq 1. Presumably, these poor fits are due to the amorphous nature of the r-ran P3HT polymer, which results in poor charge transport.¹⁰ At higher annealing temperatures (>170 °C for r-reg P3HT/C₆₀, >80 °C for r-ran P3HT/C₆₀), both sets of dark curves shift back to lower voltages, represented by a corresponding increase in *J*_o for the r-reg P3HT bilayers. Regioregular P3HT is a semicrystalline polymer, with a glass transition temperature of *T*_g ≈ −14 °C and melting temperature of *T*_m ≈ 222 °C. Regiorandom P3HT, on the other hand, is entirely amorphous, with *T*_g ≈ 10 °C. Thus, r-reg P3HT is expected to be more thermally resistant to morphological changes than r-ran P3HT.

Figure 3 summarizes the performance of these devices under 100 mW/cm² light intensity. Short circuit currents increase significantly with annealing, indicating an improvement in morphology due to mixing between the polymer and C₆₀. Again, because of its thermal properties, r-reg P3HT is more resistant to annealing, reaching a maximum of 6.6 mA/cm² at 190 °C, whereas r-ran P3HT peaks at 4.6 mA/cm² for annealing at 120 °C. Additional evidence for mixing between polymer and C₆₀ with annealing can be seen in the change in FF for the r-ran P3HT devices. Although the dark *J*–*V* curves are nonideal, we can estimate a series resistance on the order of 20 Ω·cm² at +4 V for no annealing treatment. With increasing annealing temperature, *R*_s*A* falls to as low as 2.3 Ω·cm², resulting in an improvement in device fill factor from 0.16 to as high as 0.31. Again, due to its amorphous nature, the hole mobility in r-ran P3HT bilayers is poor relative to r-reg P3HT,¹⁰ whereas mixing of C₆₀ into the r-ran P3HT film serves to reduce the effective thickness of this resistive layer and improve transport. These drastic changes in resistance are not observed in the r-reg P3HT bilayers because carrier mobilities between this polymer and C₆₀ are more balanced.^{4,57} As a consequence, FF in the r-reg P3HT/C₆₀ bilayers remains relatively constant before dropping at high annealing temperature.

For both systems, the shifts in the dark curves of Figure 2 correspond directly to increases or decreases in *V*_{oc}. From its

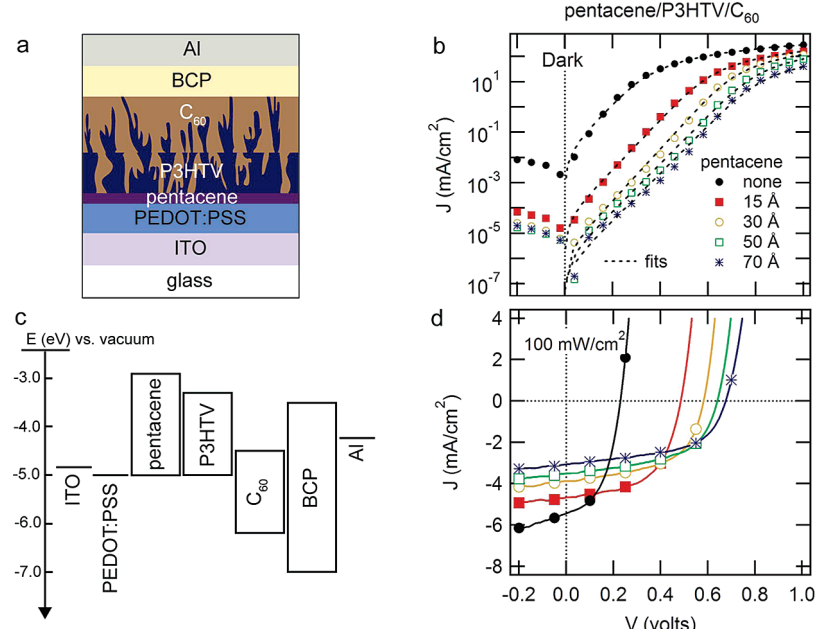


Figure 8. Pentacene/P3HTV/C₆₀ (40 nm) bilayer devices annealed at 170 °C. The pentacene layer, evaporated at the anode between PEDOT:PSS and P3HTV, was varied from 0 to 70 Å thick. P3HTV was spin-coated from a 15 mg/mL solution in 1,2-dichlorobenzene for all samples, which gave a film thickness of 23 nm for the device with no pentacene. (a) Schematic of device structure. (b) Semilog plot in the dark. Symbols are experimental data; the dashed lines represent fits to the forward current using eq 1. (c) Energy level diagram. (d) Under 100 mW/cm² light intensity.

TABLE 1: Polymer Energy Levels and V_{oc} of Unannealed Bilayers and Blends

polymer	band gap ^a (eV)	HOMO ^b (eV)	V_{oc} (V)	
			C ₆₀ bilayer ^c	PCBM blend ^d
r-ran P3HT	2.3	5.5	0.68	0.93
r-reg P3HT	1.9	5.1	0.24	0.57
P3HTV	1.7	5.0	0.23	0.48

^a Optical band gap. ^b Estimated via cyclic voltammetry. ^c ITO/PEDOT:PSS/polymer/C₆₀/BCP/Al, 100 mW/cm². ^d ITO/PEDOT:PSS/polymer:PCBM (1:1 by weight)/Ca/Al, 100 mW/cm².

TABLE 2: Solar Cell Performance and Dark Equivalent Circuit Parameters for the 170 °C Annealed Pentacene/P3HTV/C₆₀ Devices Shown in Figure 8

pentacene	none	15 Å	30 Å	50 Å	70 Å
J_{sc} (mA/cm ²)	5.25	4.77	3.79	3.42	3.13
V_{oc} (V)	0.26	0.44	0.58	0.63	0.66
FF	0.53	0.54	0.55	0.55	0.54
PCE (%)	0.73	1.12	1.19	1.19	1.11
J_o (mA/cm ²)	3.1×10^{-3}	1.4×10^{-4}	1.9×10^{-5}	6.9×10^{-7}	7.3×10^{-7}
n	1.6	1.8	1.8	1.7	1.9
R_pA ($\Omega\text{-cm}^2$)	2.0×10^4	7.0×10^5	6.4×10^6	1.2×10^7	1.4×10^7
R_sA ($\Omega\text{-cm}^2$)	2.8	2.8	2.8	3.2	3.3

initial value of 0.24 V with no annealing treatment, V_{oc} in the r-reg P3HT/C₆₀ bilayers rises with temperature up to a peak of 0.38 V at 170 °C (Figure 3a). The r-ran P3HT/C₆₀ bilayers also improve steadily with temperature, from $V_{oc} = 0.68$ V (no annealing) to 0.84 V (100 °C), (Figure 3b). These correlated shifts in J_o and V_{oc} with annealing are presumably a result of alteration in the energetics of the heterojunction between polymer and C₆₀. In addition to V_{oc} , J_o also appears to be related to the energy difference at the donor/acceptor heterojunction, HOMO_{donor} – LUMO_{acceptor}. Studies by Waldauf et al.⁵⁸ on small molecule bilayers and Rand et al.⁵⁹ on polymer bulk heterojunction blends have shown an exponential temperature dependence of J_o with barrier height equal to this donor/acceptor energy offset.

Peak power conversion efficiencies of 1.18% and 1.07% are obtained for r-reg P3HT and r-ran P3HT bilayers, respectively. Though charge transport in r-ran P3HT is relatively poor, its large oxidation potential gives a V_{oc} over 100% greater than r-reg P3HT, making the final overall PCEs comparable. For r-reg P3HT, the best annealed bilayers in Figure 3 are inferior to the best bulk heterojunction blends of r-reg P3HT with PCBM, which typically show J_{sc} in the range of 10 mA/cm² or higher and V_{oc} around 0.6 V.^{4,5,30} Blends of entirely regiorandom (i.e., 50% regioregular) P3HT and PCBM have not received much attention in the literature. Indeed, previous studies have demonstrated the importance of high regioregularity in the performance of P3HT/PCBM bulk heterojunctions.^{60,61} As a quick comparison, however, the best r-ran P3HT/C₆₀ bilayer in Figure 3b actually outperforms the best r-ran P3HT/PCBM bulk heterojunction we have made to date, which shows a maximum $J_{sc} = 2.7$ mA/cm².⁶² Granted, further improvement in r-ran P3HT/PCBM devices is likely, because a thorough optimization of this system has not been completed. Yet, this comparison shows that annealing of bilayers to form a mixed donor/acceptor heterojunction offers a potentially attractive alternative for some materials to compete with the standard method of blending polymer with PCBM in solution.

Annealing Effects: P3HTV/C₆₀. Figure 4 summarizes the device performance data for annealing experiments carried out on bilayers of P3HTV (23 nm) and C₆₀ (40 nm). Devices were annealed again for 20 min at temperatures up to 210 °C. Note that under these conditions, we do not expect any issue with thermal stability of the P3HTV film. Thermogravimetric analysis shows no weight loss up to 300 °C,⁴³ and UV-vis spectra of annealed bilayers show no drastic shifts in the polymer absorbance (Figure S2, Supporting Information).

Results here are remarkably similar to the P3HT bilayers. With no annealing, the performance of these devices is quite low, with average $J_{sc} = 2.0 \text{ mA/cm}^2$, $V_{oc} = 0.23 \text{ V}$, $FF = 0.35$, giving PCE = 0.16%. V_{oc} again initially increases with annealing temperature, up to 0.32 V, before falling suddenly at 130 °C. A steady rise occurs again beyond 130 °C, but not by enough to recover the initial loss. Short circuit currents again improve with temperature, to a maximum of 5.4 mA/cm² at 190 °C. In addition to charge collection improvement, fill factor steadily improves up to 0.53 before dropping at high temperature. Annealing also decreases R_sA , from 5.3 to 2.7 Ω·cm², further evidence that C₆₀ is improving charge transport by penetrating into the more resistive P3HTV film. EQE for these devices is plotted in Figure 5. The current contribution from both materials increases proportionately with annealing, improving from 24% to as high as 40% in the portion of the spectrum dominated by C₆₀ absorption (420 nm), and from 6% to 22% in the region dominated by P3HTV (560 nm).

The best performance in these heated bilayers ($J_{sc} = 5.3 \text{ mA/cm}^2$, $V_{oc} = 0.26 \text{ V}$, $FF = 0.53$) occurs at 170 °C, corresponding to PCE = 0.73%. This efficiency is comparable to the 0.6–0.9% efficiencies reported to date for bulk heterojunction blends of PTV polymers with PCBM.^{22–25,43} In fact, the short circuit currents and quantum efficiencies reported here are the highest observed for this polymer. The limiting factor for these bilayers is the low V_{oc} , 0.26 V, compared to V_{oc} 's near 0.50 V typically found for PTV/PCBM blends. The drop in V_{oc} at high temperatures in Figure 4 must be eliminated to achieve improved efficiencies.

C₆₀ Penetration. Penetration of C₆₀ seems the most plausible explanation for the drops in V_{oc} for all three polymers seen in Figures 3 and 4. From the trends observed in J_{sc} , FF, and R_sA , annealing at successively higher temperatures is clearly enhancing the degree of mixing between polymer and C₆₀. Conceivably, C₆₀ could penetrate all the way through the polymer film, touching the anode. If the fullerene formed continuous pathways to both electrodes, it could short the device by leaking electrons to the anode, leading to a drop in V_{oc} .

To further quantify the degree of mixing between each phase, we have imaged the surface morphology and phase contrast of annealed bilayers on glass substrates by AFM. P3HTV was spin-coated first for a thickness of ~23 nm, followed by evaporation of 40 nm C₆₀ and annealing for 20 min. Images of these films are displayed in Figure 6. With no annealing, the film surface is dominated by aggregates of C₆₀, and no phase contrast is evident. At 190–210 °C, the C₆₀ aggregates are still present, but a higher-order, micrometer scale distortion in the film becomes apparent, increasing the rms surface roughness from 1.6 nm (25 °C) to 5.2 nm (210 °C). This distortion could represent buckling of the polymer film due to an instability or dewetting at high temperature.⁶³ Most importantly, a sharp, networked phase contrast also arises at 190 °C. The phase domains become smaller and sharper in the film annealed at 210 °C, with a characteristic length scale of ~100 nm.

We conclude that annealing at 190 °C or higher is causing enough mixing of the bilayers for P3HTV to appear at the surface of the C₆₀ film. 190 °C is much higher than the drop in V_{oc} seen at 130 °C in the P3HTV/C₆₀ PV devices of Figure 4. It is important to note, however, that appearance of P3HTV at the C₆₀ surface should not pose much concern in terms of V_{oc} . Because we are using 10 nm of BCP after annealing, hole transport from P3HTV to the aluminum cathode should be effectively blocked. Nevertheless, these images provide a clue about the morphology *at the substrate* (i.e., at the ITO/PEDOT:

PSS anode of the solar cell devices). If extreme annealing causes P3HTV to appear through 40 nm of C₆₀, milder conditions will likely be sufficient for C₆₀ to percolate through 23 nm of P3HTV, especially considering the 52 °C glass transition temperature of this polymer.⁴³

In an effort to prevent full C₆₀ penetration, we have made devices with increasing P3HTV thickness, all annealed at 170 °C. Semilog plots of these devices under 100 mW/cm² light intensity are shown in Figure 7. Indeed, V_{oc} increases steadily, from 0.26 V for a 23-nm-thick P3HTV film, up to 0.46 V for an 82-nm-thick film, which is surprisingly close to the V_{oc} obtained in a P3HTV/PCBM blend (Table 1). However, FF suffers significantly with thickness, falling from 0.53 in the 23 nm film to as low as 0.31, presumably due to increased recombination in the polymer layer. J_{sc} also drops correspondingly, resulting in reduced efficiencies, 0.4–0.5%, in these thicker films.

Pentacene Blocking Layer. Rather than make the polymer film thicker, a more effective approach might be to simply block C₆₀ at the anode, similar to the way BCP blocks P3HTV at the cathode. This approach, using buffers of both organic materials and metal oxides, has previously been reported with success in both small molecule bilayer^{35,36} and polymer blend^{33,34} PV devices. To that end, we have made additional layered devices, consisting of a thin pentacene film evaporated on top of ITO/PEDOT:PSS. Pentacene was chosen because its sizable LUMO offset with C₆₀⁶⁴ should effectively block electron transport, and its HOMO level of 5.0 eV⁶⁵ should facilitate hole transport between P3HTV and PEDOT:PSS. P3HTV was then spin-coated from solution at identical concentration and spin speed, and the rest of the device was completed as already described. All devices were annealed at 170 °C after C₆₀ deposition. A schematic of this device structure and energy level diagram are provided in Figure 8.

The dark curves (Figure 8b) show significant increases in rectification and shifts toward higher voltage in the forward current with pentacene thickness. Correspondingly, under 100 mW/cm² light intensity (Figure 8d), the V_{oc} increases to as high as 0.66 V for the device with a 70 Å pentacene layer, more than 150% greater than its initial value of 0.26 V. The performance of these devices and equivalent circuit parameters are summarized in Table 2. The device with no pentacene exhibits series and shunt resistances of 2.8 Ω·cm² and 2×10^4 Ω·cm². As pentacene is added, R_sA remains essentially constant, but R_pA increases nearly 3 orders of magnitude to 1.4×10^7 Ω·cm². Meanwhile, in agreement with the increase in V_{oc} , J_o falls by well over 3 orders of magnitude. J_{sc} falls consistently with increasing pentacene thickness, from 5.3 to 3.1 mA/cm², but FF remains constant at 0.53–0.55. The drastic increase in V_{oc} more than offsets the reduction in J_{sc} , leading to improved peak power conversion efficiencies ranging from 1.11 to 1.19%, the best yet achieved for poly(phenylene vinylene) solar cells.^{22–25,43}

The reason for the drop in J_{sc} with increasing amounts of pentacene is not entirely clear. Contributions to the photocurrent from both C₆₀ and P3HTV are affected, as EQE measurements (Figure S3, Supporting Information) show a steady decrease in efficiency across the entire spectral range. The P3HTV films were all spin-coated under the same conditions from the same solution. One explanation is that wetting issues between the solution and pentacene could be causing poor P3HTV film quality or reduced thickness. Additional studies are underway to optimize the fabrication of these layers.

Conclusion

Annealing of polymer/C₆₀ devices has been shown to increase device performance by a thermally induced mixing between donor and acceptor phases combined with a forward shift in the dark J –V characteristics. All three systems exhibit a drop in V_{oc} at extreme annealing temperatures, which is attributed to penetration of C₆₀ to the ITO/PEDOT:PSS anode. We have shown this loss in V_{oc} can be eliminated either by making a thicker polymer film or including a thin C₆₀ blocking layer of pentacene at the anode. In bilayers of P3HTV/C₆₀ with a pentacene blocking layer, V_{oc} can be increased from 0.26 V to as high as 0.66 V. Optimum annealing conditions yield power conversion efficiencies as high as 1.19%. These treatments are potentially attractive as processing steps for light harvesting materials, such as new low-band gap polymers, whose performance cannot be optimized through the blending techniques common to other traditional bulk heterojunction systems.

Acknowledgment. The authors thank R. J. Holmes and J. Y. Kim for helpful discussions. This work was funded by the Initiative for Renewable Energy and the Environment (IREE) at the University of Minnesota (UMN) and the Xcel Energy Renewable Development Fund. Parts of this work were carried out in the University of Minnesota I.T. Characterization Facility, which receives partial support from NSF through the NNIN program.

Supporting Information Available: Cyclic voltammograms of polymer films, UV-vis absorbance of annealed P3HTV/C₆₀ bilayers, and EQE measurements of annealed pentacene/P3HTV/C₆₀ layered devices are included. This material is available free of charge via the Internet at <http://pubs.acs.org>.

References and Notes

- (1) Coakley, K. M.; McGehee, M. D. *Chem. Mater.* **2004**, *16*, 4533.
- (2) Brabec, C. J. *Sol. Energy Mater. Sol. Cells* **2004**, *83*, 273.
- (3) Hoth, C. N.; Schilinsky, P.; Choulis, S. A.; Brabec, C. J. *Nano Lett.* **2008**, *8*, 2806.
- (4) Li, G.; Shrotriya, V.; Huang, J.; Yao, Y.; Moriarty, T.; Emery, K.; Yang, Y. *Nat. Mater.* **2005**, *4*, 864.
- (5) Ma, W.; Yang, C.; Gong, X.; Lee, K.; Heeger, A. J. *Adv. Funct. Mater.* **2005**, *15*, 1617.
- (6) Peet, J.; Kim, J. Y.; Coates, N. E.; Ma, W. L.; Moses, D.; Heeger, A. J.; Bazan, G. C. *Nat. Mater.* **2007**, *6*, 497.
- (7) Kim, J.; Lee, K.; Coates, N.; Moses, D.; Nguyen, T.; Dante, M.; Heeger, A. *Science* **2007**, *317*, 222.
- (8) Xue, J.; Uchida, S.; Rand, B. P.; Forrest, S. R. *Appl. Phys. Lett.* **2004**, *84*, 3013.
- (9) Xue, J.; Uchida, S.; Rand, B. P.; Forrest, S. R. *Appl. Phys. Lett.* **2004**, *85*, 5757.
- (10) Sirringhaus, H.; Brown, P. J.; Friend, R. H.; Nielsen, M. M.; Bechgaard, K.; Langeveld-Voss, B. M. W.; Spiering, A. J. H.; Janssen, R. A. J.; Meijer, E. W.; Herwig, P.; de Leeuw, D. M. *Nature* **1999**, *401*, 685.
- (11) Arias, A. C.; MacKenzie, J. D.; Stevenson, R.; Halls, J. J. M.; Inbasekaran, M.; Woo, E. P.; Richards, D.; Friend, R. H. *Macromolecules* **2001**, *34*, 6005.
- (12) Shaheen, S. E.; Brabec, C. J.; Sariciftci, N. S.; Padinger, F.; Fromherz, T.; Hummelen, J. C. *Appl. Phys. Lett.* **2001**, *78*, 841.
- (13) Wienk, M. M.; Kroon, J. M.; Verhees, W. J. H.; Knol, J.; Hummelen, J. C.; van Hal, P. A.; Janssen, R. A. J. *Angew. Chem., Int. Ed.* **2003**, *42*, 3371.
- (14) van Duren, J. K. J.; Yang, X.; Loos, J.; Bulle-Lieuwma, C. W. T.; Sieval, A. B.; Hummelen, J. C.; Janssen, R. A. J. *Adv. Funct. Mater.* **2004**, *14*, 425.
- (15) Hoppe, H.; Niggemann, M.; Winder, C.; Kraut, J.; Hiesgen, R.; Hinsch, A.; Meissner, D.; Sariciftci, N. S. *Adv. Funct. Mater.* **2004**, *14*, 1005.
- (16) Schilinsky, P.; Waldauf, C.; Brabec, C. J. *Appl. Phys. Lett.* **2002**, *81*, 3885.
- (17) Dennler, G.; Scharber, M. C.; Ameri, T.; Denk, P.; Forberich, K.; Waldauf, C.; Brabec, C. J. *Adv. Mater.* **2008**, *20*, 579.
- (18) Scharber, M. C.; Mühlbacher, D.; Koppe, M.; Denk, P.; Waldauf, C.; Heeger, A. J.; Brabec, C. J. *Adv. Mater.* **2006**, *18*, 789.
- (19) Mühlbacher, D.; Scharber, M.; Morana, M.; Zhu, Z.; Waller, D.; Gaudiana, R.; Brabec, C. *Adv. Mater.* **2006**, *18*, 2884.
- (20) Blouin, N.; Michaud, A.; Leclerc, M. *Adv. Mater.* **2007**, *19*, 2295.
- (21) Blouin, N.; Michaud, A.; Gendron, D.; Wakim, S.; Blair, E.; Neagu-Plesu, R.; Belletete, M.; Durocher, G.; Tao, Y.; Leclerc, M. *J. Am. Chem. Soc.* **2008**, *130*, 732.
- (22) Smith, A. P.; Smith, R. R.; Taylor, B. E.; Durstock, M. F. *Chem. Mater.* **2004**, *16*, 4687.
- (23) Nguyen, L. H.; Günes, S.; Neugebauer, H.; Sariciftci, N. S.; Banishoeib, F.; Henkens, A.; Cleij, T.; Lutsen, L.; Vanderzande, D. *Sol. Energy Mater. Sol. Cells* **2006**, *90*, 2815.
- (24) Banishoeib, F.; Henkens, A.; Fourier, S.; Vanhooyland, G.; Breselge, M.; Manca, J.; Cleij, T. J.; Lutsen, L.; Vanderzande, D.; Nguyen, L. H.; Neugebauer, H.; Sariciftci, N. S. *Thin Solid Films* **2008**, *516*, 3978.
- (25) Girotto, C.; Cheyns, D.; Aernouts, T.; Banishoeib, F.; Lutsen, L.; Cleij, T. J.; Vanderzande, D.; Genoe, J.; Poortmans, J.; Heremans, P. *Org. Electron.* **2008**, *9*, 740.
- (26) Brabec, C. J.; Cravino, A.; Meissner, D.; Sariciftci, N. S.; Fromherz, T.; Rispens, M. T.; Sanchez, L.; Hummelen, J. C. *Adv. Funct. Mater.* **2001**, *11*, 374.
- (27) Liu, J.; Shi, Y.; Yang, Y. *Adv. Funct. Mater.* **2001**, *11*, 420.
- (28) Ramsdale, C. M.; Barker, J. A.; Arias, A. C.; MacKenzie, J. D.; Friend, R. H.; Greenham, N. C. *J. Appl. Phys.* **2002**, *92*, 4266.
- (29) Mihailitchi, V. D.; Blom, P. W. M.; Hummelen, J. C.; Rispens, M. T. *J. Appl. Phys.* **2003**, *94*, 6849.
- (30) Reese, M. O.; White, M. S.; Rumbles, G.; Ginley, D. S.; Shaheen, S. E. *Appl. Phys. Lett.* **2008**, *92*, 053307.
- (31) Frohne, H.; Shaheen, S. E.; Brabec, C. J.; Muller, D. C.; Sariciftci, N. S.; Meerholz, K. *ChemPhysChem* **2002**, *3*, 795.
- (32) Brabec, C. J.; Shaheen, S. E.; Winder, C.; Sariciftci, N. S.; Denk, P. *Appl. Phys. Lett.* **2002**, *80*, 1288.
- (33) Shrotriya, V.; Li, G.; Yao, Y.; Chu, C.; Yang, Y. *Appl. Phys. Lett.* **2006**, *88*, 073508.
- (34) Hains, A. W.; Marks, T. J. *Appl. Phys. Lett.* **2008**, *92*, 023504.
- (35) Kinoshita, Y.; Takenaka, R.; Murata, H. *Appl. Phys. Lett.* **2008**, *92*, 243309.
- (36) Li, N.; Lassiter, B. E.; Lunt, R. R.; Wei, G.; Forrest, S. R. *Appl. Phys. Lett.* **2009**, *94*, 023307.
- (37) Mayer, A. C.; Lloyd, M. T.; Herman, D. J.; Kasen, T. G.; Malliaras, G. G. *Appl. Phys. Lett.* **2004**, *85*, 6272.
- (38) Shao, Y.; Yang, Y. *Adv. Mater.* **2005**, *17*, 2841.
- (39) Shao, Y.; Sista, S.; Chu, C.; Sievers, D.; Yang, Y. *Appl. Phys. Lett.* **2007**, *90*, 103501.
- (40) Yoo, S.; Potscavage, W. J.; Domercq, B.; Han, S.; Li, T.; Jones, S. C.; Szoszkiewicz, R.; Levi, D.; Riedo, E.; Marder, S. R.; Kippelen, B. *Solid State Electron.* **2007**, *51*, 1367.
- (41) Geiser, A.; Benmansour, H.; Castro, F.; Heier, J.; Keller, B.; Mayerhofer, K. E.; Nüesch, F.; Hany, R. *Sol. Energy Mater. Sol. Cells* **2008**, *92*, 464.
- (42) Jiang, X.; Dai, J.; Wang, H.; Yan, D. *Thin Solid Films* **2008**, *516*, 6487.
- (43) Kim, J. Y.; Qin, Y.; Stevens, D. M.; Ugurlu, O.; Kalihari, V.; Hillmyer, M. A.; Frisbie, C. D. *J. Phys. Chem. C* **2009**, in press.
- (44) Qin, Y.; Hillmyer, M. A. *Macromolecules* **2009**, submitted.
- (45) Peumans, P.; Forrest, S. R. *Appl. Phys. Lett.* **2001**, *79*, 126.
- (46) Peumans, P.; Búlovic, V.; Forrest, S. R. *Appl. Phys. Lett.* **2000**, *76*, 2650.
- (47) Lloyd, M. T.; Mayer, A. C.; Tayi, A. S.; Bowen, A. M.; Kasen, T. G.; Herman, D. J.; Mourey, D. A.; Anthony, J. E.; Malliaras, G. G. *Org. Electron.* **2006**, *7*, 243.
- (48) Song, Q. L.; Li, F. Y.; Yang, H.; Wu, H. R.; Wang, X. Z.; Zhou, W.; Zhao, J. M.; Ding, X. M.; Huang, C. H.; Hou, X. Y. *Chem. Phys. Lett.* **2005**, *416*, 42.
- (49) Connolly, N. G.; Geiger, W. E. *Chem. Rev.* **1996**, *96*, 877.
- (50) Greenham, N. C.; Friend, R. H. Semiconductor Device Physics of Conjugated Polymers. In *Solid State Physics: Advances in Research and Applications*; Ehrenreich, H., Spaepen, F., Eds; Academic Press: New York, 1995; Vol. 49, pp 1–149.
- (51) Bredas, J. L.; Silbey, R.; Boudreux, D. S.; Chance, R. R. *J. Am. Chem. Soc.* **1983**, *105*, 6555.
- (52) Agrawal, A. K.; Jenekhe, S. A. *Chem. Mater.* **1996**, *8*, 579.
- (53) Chu, C.; Shrotriya, V.; Li, G.; Yang, Y. *Appl. Phys. Lett.* **2006**, *88*, 153504.
- (54) Akaike, K.; Kanai, K.; Yoshida, H.; Tsutsumi, J.; Nishi, T.; Sato, N.; Ouchi, Y.; Seki, K. *J. Appl. Phys.* **2008**, *104*, 023710.
- (55) Kippelen, B.; Yoo, S.; Haddock, J. A.; Domercq, B.; Barlow, S.; Minch, B.; Xia, W.; Marder, S. R.; Armstrong, N. R. Liquid-crystal approaches to organic photovoltaics. In *Organic Photovoltaics: Mechanisms*,

Materials, and Devices; Sun, S., Sariciftci, N. S., Eds.; CRC Press: Boca Raton, FL, 2005; pp 271–297.

(56) R_pA was estimated from the inverse slope of the dark current through 0 V, whereas R_sA , n , and J_o were fit to the forward bias characteristics assuming an infinite R_pA .

(57) Mihailetti, V. D.; Xie, H.; de Boer, B.; Popescu, L. M.; Hummelen, J. C.; Blom, P. W. M. *Appl. Phys. Lett.* **2006**, *89*, 012107.

(58) Waldau, C.; Scharber, M. C.; Schilinsky, P.; Hauch, J. A.; Brabec, C. J. *J. Appl. Phys.* **2006**, *99*, 104503.

(59) Rand, B. P.; Burk, D. P.; Forrest, S. R. *Phys. Rev. B* **2007**, *75*, 115327.

(60) Kim, Y.; Cook, S.; Tuladhar, S. M.; Choulis, S. A.; Nelson, J.; Durrant, J. R.; Bradley, D. D. C.; Giles, M.; McCulloch, I.; Ha, C.; Ree, M. *Nat. Mater.* **2006**, *5*, 197.

(61) Woo, C. H.; Thompson, B. C.; Kim, B. J.; Toney, M. F.; Frechet, J. M. J. *J. Am. Chem. Soc.* **2008**, *130*, 16324–16329.

(62) Blend device of r-ran P3HT/PCBM (1:4 by weight) spin-coated from 1,2-dichlorobenzene solution, ~54 nm thick, with Ca(20 nm)/Al (80 nm) cathode.

(63) Reiter, G. *Phys. Rev. Lett.* **1992**, *68*, 75.

(64) Kang, S. J.; Yi, Y.; Kim, C. Y.; Cho, S. W.; Noh, M.; Jeong, K.; Whang, C. N. *Synth. Met.* **2006**, *156*, 32.

(65) Harada, K.; Riede, M.; Leo, K.; Hild, O. R.; Elliott, C. M. *Phys. Rev. B* **2008**, *77*, 195212.

JP902198Y